Improved multi-position calibration for inertial measurement units

Meas. Sci. Technol. **21** (2010) 015107 (11pp) doi:10.1088/0957-0233/21/1/015107

Improved multi-position calibration for inertial measurement units

Hongliang Zhang, Yuanxin Wu, Wenqi Wu, Meiping Wu and Xiaoping Hu

Department of Automatic Control, College of Mechatronics and Automation, National University of Defense Technology, Changsha, Hunan, 410073, People's Republic of China

E-mail: hongl_zhang@hotmail.com, yuanx_wu@hotmail.com, wenqiwu_lit@hotmail.com, meipingwu@263.net and xiaopinghu@hotmail.com

Received 4 August 2009, in final form 23 September 2009
Published 23 November 2009
Online at stacks.iop.org/MST/21/015107

Abstract
Calibration of inertial measurement units (IMU) is carried out to estimate the coefficients which transform the raw outputs of inertial sensors to meaningful quantities of interest. Based on the fact that the norms of the measured outputs of the accelerometer and gyroscope cluster are equal to the magnitudes of specific force and rotational velocity inputs, respectively, an improved multi-position calibration approach is proposed. Specifically, two open but important issues are addressed for the multi-position calibration: (1) calibration of inter-triad misalignment between the gyroscope and accelerometer triads and (2) the optimal calibration scheme design. A new approach to calibrate the inter-triad misalignment is devised using the rotational axis direction measurements separately derived from the gyroscope and accelerometer triads. By maximizing the sensitivity of the norm of the IMU measurement with respect to the calibration parameters, we propose an approximately optimal calibration scheme. Simulations and real tests show that the improved multi-position approach outperforms the traditional laboratory calibration method, meanwhile relaxing the requirement of precise orientation control.

Keywords: calibration, inertial measurement units, inter-triad misalignment, optimal calibration scheme

(Some figures in this article are in colour only in the electronic version)

1. Introduction

Inertial navigation is entirely self-contained and can provide information including position, velocity and attitude at a high rate. It is now widely used as the main navigation means in missiles, aircraft, robots and other autonomous vehicles. The inertial measurement unit (IMU) generally consists of a gyroscope triad and an accelerometer triad. Their measurements, angular velocity and specific force, are integrated to yield attitude and position. As a prerequisite of inertial navigation, calibration of IMU is carried out to estimate the coefficients which transform the raw outputs of inertial sensors to meaningful quantities of interest. Traditionally, calibration is performed on a high-precision two-axis or three-axis turntable in the laboratory [1, 2], which provides precise orientation control during the calibration process. The lab calibration is cost-inefficient due to the indispensable precise turntable and the best performance achievable is fundamentally limited by the turntable precision.

Recently, a multi-position IMU calibration method was developed using the fact that the norms of the measured outputs of accelerometer and gyroscope clusters are equal to the magnitudes of specific force and rotational velocity inputs, respectively [3–10]. It can alternatively be viewed as a kind of shape-from-motion calibration method [11, 12] with magnitude constraint of motion. The major advantage is that calibration can be done without aligning the IMU to the local level frame. However, as gyroscopes and accelerometers are calibrated independently, the inter-triad misalignment estimation between the gyroscope and accelerometer triads is left as an unresolved problem [6]. Some trials have been made to attack this problem. Shin [3] concerned only scale factors and biases of gyroscopes and thus the inter-triad misalignment problem was not addressed. Zhang *et al* [8] utilized the

fact that the dot product of the gyroscope and accelerometer measurement vectors is equal to minus the dot product of the Earth's rotation rate and gravity for a static IMU, but the accuracy of gyroscopes' parameters is unacceptable because of the small magnitude of the Earth's rotation rate. Fong *et al* [7] calibrated gyroscopes by comparing the outputs of the accelerometer and the IMU orientation integration algorithm after arbitrary motions, which requires an initial rough estimate of gyroscope parameters. Another important open issue is the calibration scheme design. In order to avoid computational singularity in estimation, attitudes and rotation sequences should be designed discretely. Researchers often chose calibration schemes by experience, and the optimal design of the rotation scheme has seldom been seriously concerned to the best of our knowledge.

This paper proposes a new approach to calibrate the inter-triad misalignment between the gyroscope and accelerometer triads. A turntable is applied in the calibration process to enlarge angular velocity input, where the alignment accuracy requirement for the turntable is significantly reduced as compared with that in the traditional calibration method. When the IMU is rotated along some fixed axis, the rotational axis derived by the gyroscope triad should be equal to the corresponding quantity derived from the accelerometer triad measurements. Based on the rotational axis observations, the inter-triad misalignment between the gyroscope and accelerometer triads is successfully solved. The sensitivities of the norms of the IMU measurements with respect to the calibration parameters are investigated and we come up with an approximately optimal calibration scheme by maximizing the magnitudes of the partial derivatives with respect to the calibration parameters.

The paper is organized as follows. Section 2 presents the inertial sensor model, where the scale factors, misalignments and biases of the accelerometer and gyroscope triads are considered as the calibration parameters. Section 3 describes the separate multi-position calibrations for the gyroscope triad and the accelerometer triad, followed by the optimal calibration scheme design by maximizing the sensitivity of the measurements to calibration parameters. The method to calibrate the inter-triad misalignment between the gyroscope and accelerometer triads is given in section 4. Section 5 reports the calibration results of navigation grade IMUs through both simulations and real tests. It shows that the improved multi-position approach outperforms the traditional calibration method, with reduced alignment accuracy requirement of the turntable. Conclusions are drawn in section 6.

2. Sensor model

In this paper, we consider an IMU consisting of three almost orthogonally mounted accelerometers and three almost orthogonally mounted gyroscopes. Measurement of the accelerometer cluster can be expressed as [4, 6]

$$\tilde{\boldsymbol{s}}^a = \boldsymbol{K}_a \boldsymbol{T}_p^a \boldsymbol{s}^p + \boldsymbol{b}_a + \boldsymbol{v}_a, \tag{1}$$

where $\boldsymbol{s}^p$ denotes the input specific force expressed in platform coordinates (see below for frame definition) and $\boldsymbol{v}_a$ is the measurement noise. The scale factor matrix and bias vector of the accelerometer triad are defined, respectively, as

$$\boldsymbol{K}_a = \mathrm{diag}(k_{x_a}, k_{y_a}, k_{z_a}), \qquad \boldsymbol{b}_a = \begin{bmatrix} b_{x_a} & b_{y_a} & b_{z_a} \end{bmatrix}^T, \tag{2}$$

where k_{i_a}, b_{i_a} denote the scale factor and the bias of the ith accelerometer output. The misalignment matrix $\boldsymbol{T}_p^a$ in (1) transforms the specific force from the platform coordinates to the accelerometer sensitivity axes. Define platform coordinates p so that $\boldsymbol{x}^p$ coincides with the accelerometer sensitivity axis $\boldsymbol{x}^a$, $\boldsymbol{y}^p$ lies in the $\boldsymbol{x}^a\boldsymbol{y}^a$ plane and $\boldsymbol{z}^p$ constitutes a right-handed orthogonal frame with $\boldsymbol{x}^p$, $\boldsymbol{y}^p$. The transform matrix $\boldsymbol{T}_p^a$ can be written as [4, 6, 13]

$$\boldsymbol{T}_p^a = \begin{bmatrix} 1 & 0 & 0 \\ \boldsymbol{y}^a \cdot \boldsymbol{x}^p & \boldsymbol{y}^a \cdot \boldsymbol{y}^p & 0 \\ \boldsymbol{z}^a \cdot \boldsymbol{x}^p & \boldsymbol{z}^a \cdot \boldsymbol{y}^p & \boldsymbol{z}^a \cdot \boldsymbol{z}^p \end{bmatrix} \approx \begin{bmatrix} 1 & 0 & 0 \\ \alpha_{yz} & 1 & 0 \\ -\alpha_{zy} & \alpha_{zx} & 1 \end{bmatrix}, \tag{3}$$

where $(\boldsymbol{i}^a \cdot \boldsymbol{j}^p)$ denotes the dot product of the ith unit accelerometer sensitivity axis and the jth unit platform axis. The misalignment of accelerometers can be approximately described as three small rotation angles. α_{ij} is the rotation of the ith accelerometer sensitivity axis around the jth platform axis.

Analogously the measurement of the gyroscope cluster can be expressed as [4, 6]

$$\tilde{\boldsymbol{\omega}}_{ig}^g = \boldsymbol{K}_g \boldsymbol{T}_o^g \boldsymbol{R}_p^o \boldsymbol{\omega}_{ip}^p + \boldsymbol{b}_g + \boldsymbol{v}_g, \tag{4}$$

where $\boldsymbol{\omega}_{ip}^p$ denotes the true platform angular velocity with respect to the inertial coordinates expressed in platform coordinates, $\boldsymbol{K}_g$ is the diagonal scale factor matrix, $\boldsymbol{b}_g$ is the bias vector of the gyroscope cluster and $\boldsymbol{v}_g$ is the measurement noise. The orthogonal coordinate frame o, which is associated with gyro sensitivity axes, is defined as follows: $\boldsymbol{x}^o$ coincides with the gyroscope sensitivity axis $\boldsymbol{x}^g$, $\boldsymbol{y}^o$ lies in the $\boldsymbol{x}^g\boldsymbol{y}^g$ plane and $\boldsymbol{z}^o$ constitutes a right-handed orthogonal frame with $\boldsymbol{x}^o$, $\boldsymbol{y}^o$. The misalignment matrix of gyroscopes can be written as [4, 6, 13]

$$\boldsymbol{T}_o^g = \begin{bmatrix} 1 & 0 & 0 \\ \boldsymbol{y}^g \cdot \boldsymbol{x}^o & \boldsymbol{y}^g \cdot \boldsymbol{y}^o & 0 \\ \boldsymbol{z}^g \cdot \boldsymbol{x}^o & \boldsymbol{z}^g \cdot \boldsymbol{y}^o & \boldsymbol{z}^g \cdot \boldsymbol{z}^o \end{bmatrix} \approx \begin{bmatrix} 1 & 0 & 0 \\ \gamma_{yz} & 1 & 0 \\ -\gamma_{zy} & \gamma_{zx} & 1 \end{bmatrix}, \tag{5}$$

where γ_{ij} approximately denotes the small misalignment angle between the jth axis of the o-frame and the ith nonorthogonal gyroscope sensitivity axis. $\boldsymbol{R}_p^o$ in (4) denotes the directional cosine matrix, rotating a vector from the platform coordinates to the o-frame. Because the mounted errors between the gyroscope triad and the accelerometer triad are small, we can express $\boldsymbol{R}_p^o$ approximately as

$$\boldsymbol{R}_p^o \approx \begin{bmatrix} 1 & -\theta_z & \theta_y \\ \theta_z & 1 & -\theta_x \\ -\theta_y & \theta_x & 1 \end{bmatrix}, \tag{6}$$

where the inter-triad misalignment between the gyroscope and accelerometer triads is denoted by three small angles. θ_i is the Euler rotation angle about the i-axis.

The task of IMU calibration is to estimate such parameters as scale factors, misalignments, biases of accelerometers and gyroscopes, and the inter-triad misalignment.

3. Separate calibration of the accelerometer and gyroscope triads

In this section, the separate multi-position calibrations for the gyroscope triad and the accelerometer triad are described, followed by the optimal calibration scheme design by maximizing the sensitivity of the measurements to calibration parameters.

3.1. Separate calibration process

The fact that the norms of the measured outputs of the accelerometer and gyroscope cluster are equal to the magnitudes of specific force and applied angular velocity inputs tells us that

$$|\boldsymbol{s}^p| = \left|\left(\boldsymbol{K}_a\boldsymbol{T}_p^a\right)^{-1}(\tilde{\boldsymbol{s}}^a - \boldsymbol{b}_a)\right| = |\boldsymbol{g}|, \quad \text{for accelerometers} \tag{7}$$

and

$$\begin{aligned}\left|\boldsymbol{\omega}_{ip}^p\right| &= \left|\boldsymbol{R}_o^p\left(\boldsymbol{K}_g\boldsymbol{T}_o^g\right)^{-1}\left(\tilde{\boldsymbol{\omega}}_{ig}^g - \boldsymbol{b}_g\right)\right| \\ &= \left|\left(\boldsymbol{K}_g\boldsymbol{T}_o^g\right)^{-1}\left(\tilde{\boldsymbol{\omega}}_{ig}^g - \boldsymbol{b}_g\right)\right| = |\boldsymbol{\omega}|, \quad \text{for gyroscopes,}\end{aligned} \tag{8}$$

where $\boldsymbol{g}$ is the gravity vector, $\boldsymbol{\omega}$ is the true angular velocity of the IMU, $(\cdot)^{-1}$ denotes the inverse of a matrix and $|\cdot|$ is the norm of a vector. The above equations validate the separate calibration of the accelerometers and gyroscopes. When the accelerometer and gyroscope triads are calibrated at several different static attitudes [3, 8], $\boldsymbol{\omega} = \boldsymbol{\omega}_{ie}^n$ is the Earth's rotation rate expressed in the navigation frame. It was reported [6, 8] that the magnitude of the Earth's rotation rate is too small for the gyroscope calibration. In order to get more accurate scale factors and misalignment for gyroscopes, a turntable can be utilized to rotate IMU [6, 8]. Suppose that the rotation rate of the turntable is $\boldsymbol{\omega}_r^n$; then the true angular velocity input in (8) satisfies

$$\boldsymbol{\omega} = \boldsymbol{\omega}_{ie}^n + \boldsymbol{\omega}_r^n. \tag{9}$$

A clockwise and counter-clockwise rotation scheme is commonly applied to eliminate unknown effects of the Earth's rotation rate, so the requirements of a precisely controlled orientation of the IMU can be relaxed.

Using the mathematical models described by (7) and (8), we can calibrate the scale factors, misalignments and biases of accelerometers and gyroscopes separately. It can be achieved by minimizing a cost function [4, 5, 7]

$$\hat{\boldsymbol{\theta}} = \arg\min_{\boldsymbol{\theta}}\{L(\boldsymbol{\theta})\}, \tag{10}$$

where $\boldsymbol{\theta} = [k_{x_a}\ k_{y_a}\ k_{z_a}\ \alpha_{yz}\ \alpha_{zy}\ \alpha_{zx}\ b_{x_a}\ b_{y_a}\ b_{z_a}]^T$ for accelerometers and $\boldsymbol{\theta} = [k_{x_g}\ k_{y_g}\ k_{z_g}\ \gamma_{yz}\ \gamma_{zy}\ \gamma_{zx}\ b_{x_g}\ b_{y_g}\ b_{z_g}]^T$ for gyroscopes. The cost function for accelerometers is $L(\boldsymbol{\theta}) = \sum_{j=0}^{J_p-1}\left(|\boldsymbol{g}|^2 - \left|(\boldsymbol{s}^p)_j\right|^2\right)^2$, while for gyroscopes it is $L(\boldsymbol{\theta}) = \sum_{j=0}^{J_r-1}\left(|\boldsymbol{\omega}|^2 - \left|\left(\boldsymbol{\omega}_{ip}^p\right)_j\right|^2\right)^2$, where J_p is the number of positions and J_r the number of rotations.

Calibration can alternatively be accomplished by solving the least-squares function [3, 6, 10]

$$\boldsymbol{A}\theta = \boldsymbol{Y}, \tag{11}$$

where for accelerometers

$$\boldsymbol{\theta} = \begin{bmatrix}k_{x_a} & k_{y_a} & k_{z_a} & \alpha_{yz} & \alpha_{zy} & \alpha_{zx} & b_{x_a} & b_{y_a} & b_{z_a}\end{bmatrix}^T,$$

$$\boldsymbol{A} = \begin{bmatrix}\vdots \\ \left(\dfrac{\partial(|(\boldsymbol{s}^p)_j|^2)}{\partial\boldsymbol{\theta}}\right)^T \\ \vdots\end{bmatrix}, \qquad \boldsymbol{Y} = \begin{bmatrix}\vdots \\ |\boldsymbol{g}|^2 \\ \vdots\end{bmatrix},$$

and for gyroscopes

$$\boldsymbol{\theta} = \begin{bmatrix}k_{x_g} & k_{y_g} & k_{z_g} & \gamma_{yz} & \gamma_{zy} & \gamma_{zx} & b_{x_g} & b_{y_g} & b_{z_g}\end{bmatrix}^T,$$

$$\boldsymbol{A} = \begin{bmatrix}\vdots \\ \left(\dfrac{\partial\left(\left|\left(\boldsymbol{\omega}_{ip}^p\right)_j\right|^2\right)}{\partial\boldsymbol{\theta}}\right)^T \\ \vdots\end{bmatrix}, \qquad \boldsymbol{Y} = \begin{bmatrix}\vdots \\ |\boldsymbol{\omega}|^2 \\ \vdots\end{bmatrix}.$$

Iterative methods are commonly used to solve (10) or (11), which need an initial rough estimation of the parameters [3–7]. This paper uses the following procedure adapted from our previous work [8] to estimate the parameters that do not need any initial value. Squaring both sides of (7) gives

$$|\boldsymbol{s}^p|^2 = (\tilde{\boldsymbol{s}}^a - \boldsymbol{b}_a)^T\left[\left(\boldsymbol{K}_a\boldsymbol{T}_p^a\right)^{-1}\right]^T\left(\boldsymbol{K}_a\boldsymbol{T}_p^a\right)^{-1}(\tilde{\boldsymbol{s}}^a - \boldsymbol{b}_a) = |\boldsymbol{g}|^2. \tag{12}$$

It can be written as

$$\begin{aligned}&|\boldsymbol{g}|^2 = \\ &\left[\left(\tilde{s}_x^a\right)^2\ \left(\tilde{s}_y^a\right)^2\ \left(\tilde{s}_z^a\right)^2\ 2\tilde{s}_x^a\tilde{s}_y^a\ 2\tilde{s}_x^a\tilde{s}_z^a\ 2\tilde{s}_y^a\tilde{s}_z^a\ -2\tilde{s}_x^a\ -2\tilde{s}_y^a\ -2\tilde{s}_z^a\ 1\right] \\ &\cdot\left[m_{11}^A\ m_{22}^A\ m_{33}^A\ m_{12}^A\ m_{13}^A\ m_{23}^A\ m_{14}^A\ m_{24}^A\ m_{34}^A\ m_{44}^A\right]^T,\end{aligned} \tag{13}$$

where m_{ij}^A is defined as the element of a symmetric matrix

$$\begin{aligned}\boldsymbol{M}^A &= \begin{bmatrix}m_{11}^A & m_{12}^A & m_{13}^A & m_{14}^A \\ m_{12}^A & m_{22}^A & m_{23}^A & m_{24}^A \\ m_{13}^A & m_{23}^A & m_{33}^A & m_{34}^A \\ m_{14}^A & m_{24}^A & m_{34}^A & m_{44}^A\end{bmatrix} \\ &= \left[\left(\boldsymbol{K}_a\boldsymbol{T}_p^a\right)^{-1}\quad \left(\boldsymbol{K}_a\boldsymbol{T}_p^a\right)^{-1}\boldsymbol{b}_a\right]^T \\ &\quad\times\left[\left(\boldsymbol{K}_a\boldsymbol{T}_p^a\right)^{-1}\quad \left(\boldsymbol{K}_a\boldsymbol{T}_p^a\right)^{-1}\boldsymbol{b}_a\right].\end{aligned} \tag{14}$$

For J_p positions, we have J_p accelerometer outputs $(\tilde{\boldsymbol{s}}^a)_j$, $j = 1, \ldots, J_p$; then a least-squares method can be used to solve elements of $\boldsymbol{M}^A$. Using (14), accelerometer parameters can be determined from $\boldsymbol{M}^A$. Readers are referred to [8] for more details.

For calibrating gyroscopes, we take two steps. The first step is to calibrate scale factors and misalignment, where a clockwise and counter-clockwise rotation scheme is used to eliminate effects of the Earth's rotation rate and gyroscope bias. The second step is to estimate biases using the obtained scale factors and misalignment.

Now the first step is described as follows. When the turntable rotates clockwise along some fixed axis, the angular velocity measured by gyroscopes expressed in the o-frame is

$$\boldsymbol{\omega}_{io}^{o+}(t) = \left(\boldsymbol{K}_g\boldsymbol{T}_o^g\right)^{-1}\left(\tilde{\boldsymbol{\omega}}_{ig}^{g+}(t) - \boldsymbol{b}_g\right) = \boldsymbol{\omega}_r^o + \boldsymbol{C}_n^{o+}(t)\boldsymbol{\omega}_{ie}^n, \tag{15}$$

where $\tilde{\omega}_{ig}^{g}$ is the gyroscope raw output, the superscript '+' denotes clockwise rotation, t denotes time, ω_r^o is the constant turntable rotation rate, ω_{ie}^n is the Earth's rotation rate and C_n^o is the directional cosine matrix from the navigation frame to the o-frame. Integrating the angular velocity over the rotation period gives

$$\int_0^{t_r} \omega_{io}^{o+}(\tau)\,\mathrm{d}\tau = \left(K_g T_o^g\right)^{-1} \int_0^{t_r} \left(\tilde{\omega}_{ig}^{g+}(\tau) - b_g\right)\mathrm{d}\tau$$
$$= \omega_r^o \cdot t_r + \int_0^{t_r} C_n^{o+}(\tau)\omega_{ie}^n\,\mathrm{d}\tau \tag{16}$$

where t_r is the time length of rotation.

Analogously, when the turntable rotates counter-clockwise along the same axis with the same rate, integration of the measured angular velocity over the same time length is

$$\int_0^{t_r} \omega_{io}^{o-}(\tau)\,\mathrm{d}\tau = \left(K_g T_o^g\right)^{-1} \int_0^{t_r} \left(\tilde{\omega}_{ig}^{g-}(\tau) - b_g\right)\mathrm{d}\tau$$
$$= -\omega_r^o \cdot t_r + \int_0^{t_r} C_n^{o-}(\tau)\omega_{ie}^{\mathrm{n}}\,\mathrm{d}\tau, \tag{17}$$

where the superscript '−' denotes the counter-clockwise rotation. Note that $\omega_r^o \cdot t_r$ is the table's rotation angle vector during the interval that is directly accessible from the table display. For approximately even turntable rotation, it should be precisely expressed as $\int_0^{t_r} \omega_r^o\,\mathrm{d}\tau$ instead, which does not alter the following development. The time-integrating strategy relaxes the requirement of constant ω_r^o as only the rotation angle vector really matters.

Subtracting (17) from (16), we eliminate the effect of the Earth's rotation rate and the gyroscope bias and get

$$\int_0^{t_r} \omega_{io}^{o+}(\tau)\,\mathrm{d}\tau - \int_0^{t_r} \omega_{io}^{o-}(\tau)\,\mathrm{d}\tau = \left(K_g T_o^g\right)^{-1}\left[\int_0^{t_r} \tilde{\omega}_{ig}^{g+}(\tau)\,\mathrm{d}\tau - \int_0^{t_r} \tilde{\omega}_{ig}^{g-}(\tau)\,\mathrm{d}\tau\right] = 2\omega_r^o \cdot t_r. \tag{18}$$

Taking the norm of (18) yields

$$\left|\left(K_g T_o^g\right)^{-1}\left[\int_0^{t_r} \tilde{\omega}_{ig}^{g+}(\tau)\,\mathrm{d}\tau - \int_0^{t_r} \tilde{\omega}_{ig}^{g-}(\tau)\,\mathrm{d}\tau\right]\right| = 2\left|\omega_r^o\right| \cdot t_r. \tag{19}$$

Squaring the norm and reorganizing the terms yield

$$\left[\int_0^{t_r} \tilde{\omega}_{ig}^{g+}(\tau)\,\mathrm{d}\tau - \int_0^{t_r} \tilde{\omega}_{ig}^{g-}(\tau)\,\mathrm{d}\tau\right]^T \left[\left(K_g T_o^g\right)^{-1}\right]^T \left(K_g T_o^g\right)^{-1} \times \left[\int_0^{t_r} \tilde{\omega}_{ig}^{g+}(\tau)\,\mathrm{d}\tau - \int_0^{t_r} \tilde{\omega}_{ig}^{g-}(\tau)\,\mathrm{d}\tau\right] = 4\left|\omega_r^o\right|^2 \cdot t_r^2. \tag{20}$$

It can be written as

$$4\left|\omega_r^o\right|^2 \cdot t_r^2 = \left[\left(\phi_x^g\right)^2 \quad \left(\phi_y^g\right)^2 \quad \left(\phi_z^g\right)^2 \quad 2\phi_x^g\phi_y^g \quad 2\phi_x^g\phi_z^g \quad 2\phi_y^g\phi_z^g\right] \cdot \left[m_{11}^G \quad m_{22}^G \quad m_{33}^G \quad m_{12}^G \quad m_{13}^G \quad m_{23}^G\right]^T, \tag{21}$$

where $\phi^g = \int_0^{t_r} \tilde{\omega}_{ig}^{g+}(\tau)\,\mathrm{d}\tau - \int_0^{t_r} \tilde{\omega}_{ig}^{g-}(\tau)\,\mathrm{d}\tau$ and m_{ij}^G is the element of a symmetric matrix

$$M^G = \begin{bmatrix} m_{11}^G & m_{12}^G & m_{13}^G \\ m_{12}^G & m_{22}^G & m_{23}^G \\ m_{13}^G & m_{23}^G & m_{33}^G \end{bmatrix} = \left[\left(K_g T_o^g\right)^{-1}\right]^T \left(K_g T_o^g\right)^{-1}. \tag{22}$$

Similar to the accelerometer calibration, for J_r rotations, we have J_r integrations of gyroscope outputs subtraction $(\phi^g)_j$, $j = 1, \ldots, J_r$, and a least-squares method can be used to solve the elements of M^G. Then scale factors and misalignments can be determined from (22).

The second step is to estimate gyroscope biases. For a static IMU, (8) becomes

$$\left|\omega_{ip}^p\right| = \left|R_o^p\left(K_g T_o^g\right)^{-1}\left(\tilde{\omega}_{ig}^g - b_g\right)\right| = \left|\left(K_g T_o^g\right)^{-1}\left(\tilde{\omega}_{ig}^g - b_g\right)\right| = \left|\omega_{ie}^n\right|. \tag{23}$$

Squaring (23) gives

$$\left[\left(K_g T_o^g\right)^{-1}\tilde{\omega}_{ig}^g\right]^T\left[\left(K_g T_o^g\right)^{-1}\tilde{\omega}_{ig}^g\right] - 2\left[\left(K_g T_o^g\right)^{-1}\tilde{\omega}_{ig}^g\right]^T\left(K_g T_o^g\right)^{-1} b_g + \left[\left(K_g T_o^g\right)^{-1} b_g\right]^T\left[\left(K_g T_o^g\right)^{-1} b_g\right] = \left|\omega_{ie}^n\right|^2. \tag{24}$$

Suppose we get gyroscope outputs $\left(\tilde{\omega}_{ig}^g\right)_{j_1}$ and $\left(\tilde{\omega}_{ig}^g\right)_{j_2}$ for two different static positions; then we have by subtracting the two equations

$$2\left\{\left(K_g T_o^g\right)^{-1}\left[\left(\tilde{\omega}_{ig}^g\right)_{j_1} - \left(\tilde{\omega}_{ig}^g\right)_{j_2}\right]\right\}^T\left(K_g T_o^g\right)^{-1} b_g = \left[\left(K_g T_o^g\right)^{-1}\left(\tilde{\omega}_{ig}^g\right)_{j_1}\right]^T\left[\left(K_g T_o^g\right)^{-1}\left(\tilde{\omega}_{ig}^g\right)_{j_1}\right] - \left[\left(K_g T_o^g\right)^{-1}\left(\tilde{\omega}_{ig}^g\right)_{j_2}\right]^T\left[\left(K_g T_o^g\right)^{-1}\left(\tilde{\omega}_{ig}^g\right)_{j_2}\right]. \tag{25}$$

With the obtained scale factors and misalignment, a least-squares method can be used to calibrate biases for more static positions.

3.2. Optimal calibration scheme

In order to avoid computational singularity in estimation, the calibration scheme should be carefully designed. Generally speaking, at least nine different attitudes for accelerometers and at least nine different rotations for gyroscopes are required in calibration as there are nine unknown parameters in both the accelerometer triad and the gyroscope triad [3, 4, 6, 8]. In reality, more positions are desired to get numerically reliable results. Then a question arises: what scheme is the best for calibration? The optimal scheme not only makes all the calibration parameters identifiable, but also maximizes their numerical accuracy.

An easy criterion used in the design of optimal input for parameter identification is to maximize the sensitivity of measurement to the unknown parameters [14–17]. In the current context, the calibration scheme determines the IMU input, and the measurements are the norms of the accelerometer and gyroscope meaningful measurements (7) and (8). The optimal calibration scheme is proposed by maximizing the sensitivity of the measurement norms with respect to the calibration parameters.

Squaring both sides of (7) gives

$$\left|s^p\right|^2 = \left(\tilde{s}^a - b_a\right)^T\left[\left(K_a T_p^a\right)^{-1}\right]^T\left(K_a T_p^a\right)^{-1}\left(\tilde{s}^a - b_a\right) = |g|^2. \tag{26}$$

Table 1. Approximately optimal nine attitudes for calibrating accelerometers.

Posture no.	1	2	3
Description	*x*-upward	*x*-downward	*y*-upward
Illustration			
Posture no.	4	5	6
Description	*y*-downward	*z*-upward	*z*-downward
Illustration	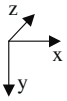		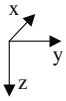
Posture no.	7	8	9
Description	*x*-east, *y*-north-upward with 45° pitch, *z*-south-upward with 45° pitch	*y*-east, *z*-north-upward with 45° pitch, *x*-south-upward with 45° pitch	*z*-east, *x*-north-upward with 45° pitch, *y*-south-upward with 45° pitch
Illustration	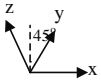	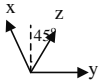	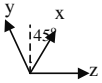

Substituting (2) and (3) into (26) and reorganizing terms yields

$$\begin{aligned}|\boldsymbol{s}^p|^2 &= \left(s_x^p\right)^2 + \left(s_y^p\right)^2 + \left(s_z^p\right)^2 \\ &= \left[\frac{1}{k_{x_a}}\left(\tilde{s}_x^a - b_{x_a}\right)\right]^2 + \left[-\frac{\alpha_{yz}}{k_{x_a}}\left(\tilde{s}_x^a - b_{x_a}\right) + \frac{1}{k_{y_a}}\left(\tilde{s}_y^a - b_{y_a}\right)\right]^2 \\ &\quad + \left[\frac{\alpha_{zy} + \alpha_{yz}\alpha_{zx}}{k_{x_a}}\left(\tilde{s}_x^a - b_{x_a}\right)\right. \\ &\quad \left. - \frac{\alpha_{zx}}{k_{y_a}}\left(\tilde{s}_y^a - b_{y_a}\right) + \frac{1}{k_{z_a}}\left(\tilde{s}_z^a - b_{z_a}\right)\right]^2. \end{aligned} \tag{27}$$

Let us write

$$\boldsymbol{s}^a = \begin{bmatrix} s_x^a & s_y^a & s_z^a \end{bmatrix}^T = (\boldsymbol{K}_a)^{-1}(\tilde{\boldsymbol{s}}^a - \boldsymbol{b}_a). \tag{28}$$

Taking the partial derivatives of (27) with respect to the scale factor k_{x_a}, we have

$$\begin{aligned}\frac{\partial|\boldsymbol{s}^p|^2}{\partial k_{x_a}} &= -\frac{2}{k_{x_a}^2}\left(\tilde{s}_x^a - b_{x_a}\right)\left[s_x^p - \alpha_{yz}s_y^p + (\alpha_{zy} + \alpha_{yz}\alpha_{zx})s_z^p\right] \\ &= -\frac{2}{k_{x_a}}s_x^a\left[s_x^p - \alpha_{yz}s_y^p + \left(\alpha_{zy} + \alpha_{yz}\alpha_{zx}\right)s_z^p\right]. \end{aligned} \tag{29}$$

Analogously we get

$$\frac{\partial|\boldsymbol{s}^p|^2}{\partial k_{y_a}} = -\frac{2}{k_{y_a}}s_y^a\left(s_y^p - \alpha_{zx}s_z^p\right), \quad \frac{\partial|\boldsymbol{s}^p|^2}{\partial k_{z_a}} = -\frac{2}{k_{z_a}}s_z^a s_z^p \tag{30}$$

$$\begin{aligned}&\frac{\partial|\boldsymbol{s}^p|^2}{\partial \alpha_{yz}} = -2s_x^a\left(s_y^p - \alpha_{zx}s_z^p\right), \quad \frac{\partial|\boldsymbol{s}^p|^2}{\partial \alpha_{zy}} = 2s_x^a s_z^p, \\ &\frac{\partial|\boldsymbol{s}^p|^2}{\partial \alpha_{zx}} = -2s_z^p\left(s_y^a - \alpha_{yz}s_x^a\right)\end{aligned} \tag{31}$$

$$\begin{aligned}&\frac{\partial|\boldsymbol{s}^p|^2}{\partial b_{x_a}} = -\frac{2}{k_{x_a}}\left[s_x^p - \alpha_{yz}s_y^p + (\alpha_{zy} + \alpha_{yz}\alpha_{zx})s_z^p\right], \\ &\frac{\partial|\boldsymbol{s}^p|^2}{\partial b_{y_a}} = -\frac{2}{k_{y_a}}\left(s_y^p - \alpha_{zx}s_z^p\right), \quad \frac{\partial|\boldsymbol{s}^p|^2}{\partial b_{z_a}} = -\frac{2}{k_{z_a}}s_z^p.\end{aligned} \tag{32}$$

Ignoring the small quantity terms containing α_{ij} $(i, j = x, y, z)$, we can write (29)–(32) as

$$\frac{\partial|\boldsymbol{s}^p|^2}{\partial k_{i_a}} = -\frac{2}{k_{i_a}}s_i^a s_i^p \tag{33}$$

$$\frac{\partial|\boldsymbol{s}^p|^2}{\partial \alpha_{yz}} = -2s_x^a s_y^p, \quad \frac{\partial|\boldsymbol{s}^p|^2}{\partial \alpha_{zy}} = 2s_x^a s_z^p, \quad \frac{\partial|\boldsymbol{s}^p|^2}{\partial \alpha_{zx}} = -2s_y^a s_z^p \tag{34}$$

$$\frac{\partial|\boldsymbol{s}^p|^2}{\partial b_{i_a}} = -\frac{2}{k_{i_a}}s_i^p, \tag{35}$$

where $i = x, y, z$.

As α_{ij} in $\boldsymbol{T}_p^a$ is small, s_i^a defined in (28) is approximately equal to s_i^p for $i = x, y, z$. From (33) and (35), when the i-accelerometer points up or down vertically (parallel to the gravity vector), the magnitudes of $\frac{\partial|\boldsymbol{s}^p|^2}{\partial k_{i_a}}$ and $\frac{\partial|\boldsymbol{s}^p|^2}{\partial b_{i_a}}$ are maximized, i.e. the sensitivities of specific force norm with respect to the scale factor and bias of the ith accelerometer are maximized. And from (34), when the gravity vector lies in the plane spanned by the ith and jth accelerometer sensitive axes and forms 45° or 135° angle with them, the magnitude of $\left(\pm 2s_i^a s_j^p\right)$ is maximized, i.e. the sensitivity of the specific force norm with respect to the associated misalignment angle α is maximized. By maximizing the sensitivity of the norms with respect to the calibration parameters, we get an approximately optimal scheme containing nine attitudes for calibrating accelerometers: six attitudes with sensitive axes of accelerometers pointing up and down vertically and three attitudes with the gravity vector lying in the plane spanned by any two accelerometer sensitive axes and forming 45° or 135° angle with them. An example of the nine positions is listed in table 1, which are part of the orientations (no. 1–7, 9, 11) proposed in [13]. A comparison between the proposed calibration scheme and that in [13] is given in section 5.1.

Analogously, denote

$$\boldsymbol{\sigma}^o = \left(\boldsymbol{K}_g \boldsymbol{T}_o^g\right)^{-1}\left[\int_0^{t_r} \tilde{\omega}_{ig}^{g+}(\tau)\,\mathrm{d}\tau - \int_0^{t_r} \tilde{\omega}_{ig}^{g-}(\tau)\,\mathrm{d}\tau\right]$$
$$\boldsymbol{\sigma}^g = (K_g)^{-1}\left[\int_0^{t_r} \tilde{\omega}_{ig}^{g+}(\tau)\,\mathrm{d}\tau - \int_0^{t_r} \tilde{\omega}_{ig}^{g-}(\tau)\,\mathrm{d}\tau\right]. \tag{36}$$

Taking partial derivatives of $|\boldsymbol{\sigma}^o|^2$ with respect to the scale factors k_{i_g} and the misalignment γ_{ij} $(i, j = x, y, z)$, and ignoring the small quantity terms containing γ_{ij}, we have

$$\frac{\partial|\boldsymbol{\sigma}^o|^2}{\partial k_{i_g}} = -\frac{2}{k_{i_g}}\sigma_i^g\sigma_i^o \tag{37}$$

$$\frac{\partial|\boldsymbol{\sigma}^o|^2}{\partial\gamma_{yz}} = -2\sigma_x^g\sigma_y^o, \quad \frac{\partial|\boldsymbol{\sigma}^o|^2}{\partial\gamma_{zy}} = 2\sigma_x^g\sigma_z^o,$$
$$\frac{\partial|\boldsymbol{\sigma}^o|^2}{\partial\gamma_{zx}} = -2\sigma_y^g\sigma_z^o, \tag{38}$$

where $i = x, y, z$.

Maximizing the magnitudes of the partial derivatives, we get the approximately optimal scheme for calibrating scale factors and misalignment of gyroscopes: three rotations (clockwise and counter-clockwise) along three sensitive axes of gyroscopes, three rotations (clockwise and counter-clockwise) such that the rotation axis lies in the plane spanned by any two gyroscope sensitive axes and forms 45° or 135° angle with them.

4. Calibration of inter-triad misalignment

In this section, we calibrate the inter-triad misalignment $\boldsymbol{R}_p^o$ between the gyroscope and accelerometer triads. If we can find two linearly independent vectors $\boldsymbol{l}_1$ and $\boldsymbol{l}_2$, and know their expressions both in the p-frame and in the o-frame, i.e.

$$l_i^o = \boldsymbol{R}_p^o \boldsymbol{l}_i^p, \qquad i = 1, 2, \tag{39}$$

then the attitude matrix $\boldsymbol{R}_p^o$ can be determined uniquely [18]:

$$\boldsymbol{R}_p^o = \begin{bmatrix} l_1^o & l_2^o & l_1^o \times l_2^o \end{bmatrix}\begin{bmatrix} l_1^p & l_2^p & l_1^p \times l_2^p \end{bmatrix}^{-1}, \tag{40}$$

where '$\times$' denotes cross product.

We take the unit rotational axis as the vector $\boldsymbol{l}$ in (39) and (40). When the IMU rotates along two different fixed axes, gyroscope outputs can be used to determine the unit rotational axes $\boldsymbol{l}_i^o$ $(i = 1, 2)$. If $\boldsymbol{l}_i^p$ $(i = 1, 2)$ can be derived from accelerometer outputs, then $\boldsymbol{R}_p^o$ can be estimated from (40).

From (18), the unit rotational axis in the o-frame is

$$\boldsymbol{l}^o = \frac{\boldsymbol{\omega}_r^o}{|\boldsymbol{\omega}_r^o|} = \frac{\left(\boldsymbol{K}_g \boldsymbol{T}_o^g\right)^{-1}\left[\int_0^{t_r} \tilde{\omega}_{ig}^{g+}(\tau)\,\mathrm{d}\tau - \int_0^{t_r} \tilde{\omega}_{ig}^{g-}(\tau)\,\mathrm{d}\tau\right]}{\left|\left(\boldsymbol{K}_g \boldsymbol{T}_o^g\right)^{-1}\left[\int_0^{t_r} \tilde{\omega}_{ig}^{g+}(\tau)\,\mathrm{d}\tau - \int_0^{t_r} \tilde{\omega}_{ig}^{g-}(\tau)\,\mathrm{d}\tau\right]\right|}. \tag{41}$$

Also in clockwise or counter-clockwise rotation, the specific force measured by accelerometers satisfies (figure 1)

$$[\boldsymbol{s}^p(t)]^T\boldsymbol{l}^p = [-\boldsymbol{g}^p + \boldsymbol{f}^p(t)]^T\boldsymbol{l}^p = (-\boldsymbol{g}^p)^T\boldsymbol{l}^p = \kappa, \tag{42}$$

where $\boldsymbol{s}^p(t)$ is the specific force at time t, $\boldsymbol{l}^p$ is the rotational axis expressed in the platform coordinates, $\boldsymbol{g}^p$ is the gravity vector in the p-frame, κ is a constant and $\boldsymbol{f}^p(t)$ is the centripetal acceleration caused by the lever arm between the accelerometer center and the rotational axis. Equation (42) holds because the centripetal acceleration is always perpendicular to the rotational axis, i.e.

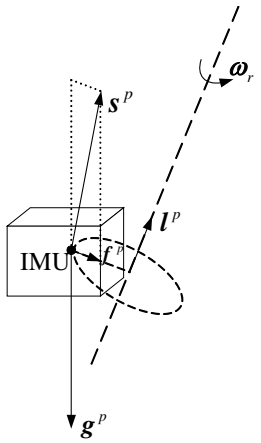

Figure 1. IMU rotation and specific force.

$$(\boldsymbol{f}^p(t))^T\boldsymbol{l}^p = 0. \tag{43}$$

We can rewrite (42) as

$$[(\boldsymbol{s}^p(t))^T \quad -1]\begin{bmatrix}\boldsymbol{l}^p \\ \kappa\end{bmatrix} = 0. \tag{44}$$

When the rotation direction is not parallel to the gravity vector, we have $\mathrm{rank}\left\{\begin{bmatrix}(\boldsymbol{s}^p(t_0))^T & -1 \\ (\boldsymbol{s}^p(t_1))^T & -1 \\ \vdots & \vdots\end{bmatrix}\right\} = 3$. Define

$$\varsigma = \begin{bmatrix}\varsigma_1 \\ \varsigma_2 \\ \varsigma_3 \\ \varsigma_4\end{bmatrix} = \begin{bmatrix}\boldsymbol{l}^p \\ \kappa\end{bmatrix}. \tag{45}$$

Then from (44), we have

$$\boldsymbol{A}\varsigma = 0 \cdot \varsigma = 0, \tag{46}$$

where $\boldsymbol{A} = \begin{bmatrix}(\boldsymbol{s}^p(t_0))^T & -1 \\ (\boldsymbol{s}^p(t_1))^T & -1 \\ \vdots & \vdots\end{bmatrix}$. Equation (46) implies that ς is the eigenvector of $\boldsymbol{A}$ belonged to zero eigenvalue. And the unit rotational axis $\boldsymbol{l}^p$ can be derived as

$$\boldsymbol{l}^p = \frac{1}{\sqrt{\varsigma_1^2 + \varsigma_2^2 + \varsigma_3^2}}\begin{bmatrix}\varsigma_1 \\ \varsigma_2 \\ \varsigma_3\end{bmatrix}. \tag{47}$$

Choose two different rotational axes, $\boldsymbol{R}_p^o$ can be readily derived from (40). More accurate $\boldsymbol{R}_p^o$ can be obtained by more rotational axes using a method similar to attitude determination [18].

From the norm equations (7) and (8) and the rotational axes measurements (41) and (47), it is not required to align the IMU to the local level frame. Systematically, gyroscope parameters are only contaminated by turntable rotation instability. For example, the scale factor error is proportional to the turn angle error. Accelerometer parameters are almost independent of turntable errors. The inter-triad

Table 2. A set of simulation results for an IMU consisting of three gyroscopes with noise 0.1° h^{-1} $Hz^{-1/2}$ and three accelerometers with noise 500 μg $Hz^{-1/2}$.

	Parameters set	Parameters calibrated	Calibration errors
Scale factors of accelerometers ($k_{x_a}, k_{y_a}, k_{z_a}$)	100 100 100	100.001 336 99.999 635 100.000 073	13.36 ppm −3.65 ppm 0.73 ppm
Misalignment of the acclerometer triad, arc-sec ($\alpha_{yz}, \alpha_{zy}, \alpha_{zx}$)	−180 60 330	−168.48 31.91 311.26	11.52 −28.09 −18.74
Biases of accelerometers, μg ($b_{x_a}, b_{y_a}, b_{z_a}$)	612.24 −2040.82 −1020.41	599.96 −2097.56 −1079.73	−12.28 −56.74 −59.32
Scale factors of gyroscopes ($k_{x_g}, k_{y_g}, k_{z_g}$)	1×10^6 1×10^6 1×10^6	$1.000\,000\,74 \times 10^6$ $0.999\,999\,94 \times 10^6$ $0.999\,999\,79 \times 10^6$	0.74 ppm −0.06 ppm −0.21 ppm
Misalignment of the gyroscope triad, arc-sec ($\gamma_{yz}, \gamma_{zy}, \gamma_{zx}$)	300 −360 48	299.77 −359.55 47.63	−0.23 0.45 −0.37
Biases of gyroscopes, ° h^{-1} ($b_{x_g}, b_{y_g}, b_{z_g}$)	0.12 −0.20 0.05	0.1192 −0.2170 0.0534	−0.0008 −0.0170 0.0034
Inter-triad misalignment angles between the gyroscope and accelerometer triads, arc-sec ($\theta_x, \theta_y, \theta_z$)	−600 120 −420	−581.48 120.83 −415.01	18.52 0.83 4.99

Table 3. Calibration errors of 500 Monte Carlo simulations for IMU consisting of three gyroscopes with noise 0.1° h^{-1} $Hz^{-1/2}$ and three accelerometers with noise 500 μg $Hz^{-1/2}$.

Parameters calibrated	Standard deviation errors
Scale factors of accelerometers, ppm ($k_{x_a}, k_{y_a}, k_{z_a}$)	34.92, 35.92, 36.90
Misalignment of accelerometer triad, arc-sec ($\alpha_{yz}, \alpha_{zy}, \alpha_{zx}$)	26.57, 28.66, 27.96
Biases of accelerometers, μg ($b_{x_a}, b_{y_a}, b_{z_a}$)	32.84, 36.20, 35.86
Scale factors of gyroscopes, ppm ($k_{x_g}, k_{y_g}, k_{z_g}$)	0.23, 0.23, 0.25
Misalignment of gyroscope triad, arc-sec ($\gamma_{yz}, \gamma_{zy}, \gamma_{zx}$)	0.11, 0.11, 0.11
Biases of gyroscopes, ° h^{-1} ($b_{x_g}, b_{y_g}, b_{z_g}$)	0.0081, 0.0103, 0.0087
Inter-triad misalignment angles between gyroscope and accelerometer triads, arc-sec ($\theta_x, \theta_y, \theta_z$)	26.16, 28.89, 29.45

misalignment error comes from the physical rotational axis disturbance of the turntable. In contrast, the fully controlled traditional laboratory method is more inherently limited by the turntable precision. Reference information errors due to an imprecise turntable (such as angle position error, axes non-orthogonality error and rate instability) are propagated to all calibration parameters. The improved multi-position calibration approach relaxes the accuracy requirement of the turntable, and hopefully can yield more accurate calibration results with the same turntable.

5. Simulations and real tests

5.1. Simulations

We assume an arc-sec grade turntable to calibrate IMUs using the proposed method. The turntable rotation angles are set with 2 arc-sec errors (1σ). We assume that the average lever arm between the accelerometer center and the table rotational axis is 5 cm and take into account the perturbed acceleration of magnitude 50 μg (1σ). The IMU consists of three gyroscopes with noise 0.1° h^{-1} $Hz^{-1/2}$ and three accelerometers with noise 500 μg $Hz^{-1/2}$, being sampled at 100 Hz. The approximately optimal calibration scheme described in section 3 is used. Data are collected for 100 s at each position for the accelerometer calibration. When calibrating gyroscopes and inter-triad misalignment, the turntable rotates at 10° s^{-1} for 180 s. A set of calibration results is shown in table 2, as well as the true values and calibration errors.

It shows that the calibration errors of the accelerometer and gyroscope biases are about 50 μg and 0.01° h^{-1}, respectively. Other accelerometer calibration errors are less than 15 ppm for scale factors, and less than 30 arc-sec for misalignment. The accuracy of gyroscope scale factors and misalignment is much higher than that of the accelerometer: less than 1 ppm for the scale factor and 0.5 arc-sec for misalignment. The inter-triad misalignment angles' errors are less than 20 arc-sec. The standard deviations of calibration errors in 500 Monte Carlo simulations (with the same settings) are shown in table 3.

Table 4. Calibration errors of 500 Monte Carlo simulations for IMU consisting of three gyroscopes with noise 0.03° h^{-1} $Hz^{-1/2}$ and three accelerometers with noise 100 μg $Hz^{-1/2}$.

Parameters calibrated	Standard deviation errors
Scale factors of accelerometers, ppm $\left(k_{x_a}, k_{y_a}, k_{z_a}\right)$	7.22, 7.13, 7.21
Misalignment of accelerometer triad, arc-sec $\left(\alpha_{yz}, \alpha_{zy}, \alpha_{zx}\right)$	5.46, 5.54, 5.27
Biases of accelerometers, μg $\left(b_{x_a}, b_{y_a}, b_{z_a}\right)$	7.37, 7.32, 6.98
Scale factors of gyroscopes, ppm $\left(k_{x_g}, k_{y_g}, k_{z_g}\right)$	0.18, 0.19, 0.19
Misalignment of gyroscope triad, arc-sec $(\gamma_{yz}, \gamma_{zy}, \gamma_{zx})$	0.09, 0.09, 0.09
Biases of gyroscopes, ° h^{-1} $\left(b_{x_g}, b_{y_g}, b_{z_g}\right)$	0.0024, 0.0033, 0.0025
Inter-triad misalignment angles between gyroscope and accelerometer triads, arc-sec $(\theta_x, \theta_y, \theta_z)$	5.30, 5.56, 5.45

Table 4 shows the standard deviations of parameter errors in 500 Monte Carlo simulations for a gyroscope noise 0.03° h^{-1} $Hz^{-1/2}$ and an accelerometer noise 100 μg $Hz^{-1/2}$. Other settings stay the same. Gyroscope scale factors and misalignment in table 4 are a little more precise than those in table 3. Gyroscope bias error is about 0.003° h^{-1}. Other parameters largely depend on the precision of the accelerometer. The reason may be that we use the local gravity (1 g) as the accelerometer input, while the gyroscope input can be given as large as the turntable can. Since the accelerometer accuracy is five times higher (100 μg $Hz^{-1/2}$ versus 500 μg $Hz^{-1/2}$), accelerometer and inter-triad misalignment errors are about one fifth of those in table 3. The calibration accuracy improves along with the increased quality of inertial sensors.

From the derivation of optimal calibration, the sensitivity of specific force norm with respect to misalignment angles is maximized at no. 2, 4, 6, 8, 10, 12–18 orientations described in [13]. It suggests that incorporating these orientations would significantly enhance misalignment estimation. Some results of 500 Monte Carlo simulations for accelerometer calibration are shown in table 5. Computational singularity appears when only no. 8, 10, 12–18 orientations are used. More positions lead to more accurate results. When all 18 orientations are used, misalignment calibration precision is improved about 2.7 times over that for the proposed nine positions (no. 1–7, 9, 11), while the scale factor and bias are just improved about 1.35 and 1.75 times, respectively. It shows that the preferred scheme is to first of all include the nine proposed orientations and then consider adding more to further improve the results.

5.2. Real tests

A navigation grade IMU was calibrated in the laboratory consisting of three laser gyroscopes (0.03° h^{-1} $Hz^{-1/2}$) and three quartz accelerometers (100 μg $Hz^{-1/2}$), using a turntable with about 2 arc-sec accuracy (1σ) (figure 2). The IMU is warmed up for over 4 h before calibration. Data are sampled at 100 Hz. Both a traditional calibration method and the proposed approach were performed in the laboratory. The traditional method takes a 24-position scheme [19] for accelerometer parameters and gyroscope biases and a three-axis rotation scheme for gyroscope scale factors and misalignment. In the 24-position scheme, the X, Y and Z axes of the platform coordinates are set vertically upward and downward, respectively, and when the ith axis is vertically upward or downward, the jth ($j \neq i$) axis is set to the north, west, south and east directions in order. The three-axis rotation scheme uses clockwise and counter-clockwise rotations at ±10° s^{-1} along the X, Y and Z axes of the platform coordinates. In both methods, the IMU stays for 100 s at each still position for accelerometer calibration and the rotation rate was set to 10° s^{-1} for the gyroscope and inter-triad misalignment calibration. Table 6 gives the calibration results of both calibration methods as well as their discrepancies.

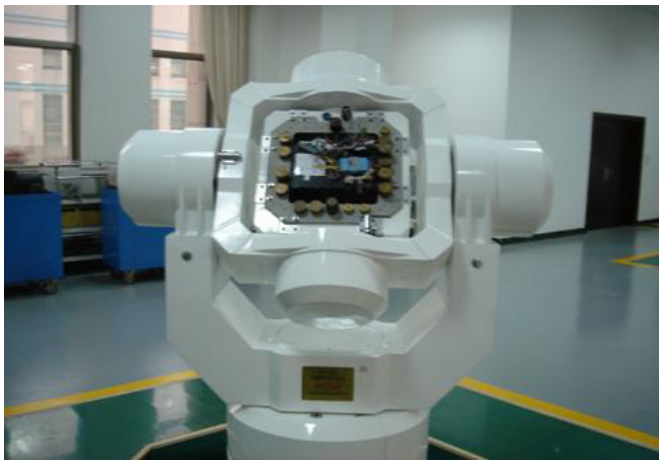

Figure 2. Calibration turntable.

Two kinds of evaluation tests were performed in the laboratory: static measurement tests and inertial navigation tests. In static measurement tests, the IMU stays static at 48 positions, and the specific force and angular velocity measurements are collected. Ideally, the specific force and angular velocity should be equal to the gravity and the Earth's rotation rate, respectively, in magnitude. Norm errors of specific force measurement are shown in figure 3, with standard deviation 13.28 μg for the traditional method and 4.94 μg for the proposed method. Norm errors of angular velocity measurement are shown in figure 4. The standard deviations are 0.0434° h^{-1} for both methods.

In inertial navigation tests, the IMU was fixed on the turntable for inertial navigation operation. Two groups of navigation tests were performed: test I and test II. In both

Table 5. Standard calibration deviations errors of 500 Monte Carlo simulations for accelerometer triad with noise 500 μg $Hz^{-1/2}$.

Orientations in reference [13] for calibration	No. 1–7, 9, 11 (the proposed approximately optimal nine positions)	No. 8, 10, 12–18	No. 1–18
Scale factors of accelerometers (ppm)	34.11, 34.67, 35.82	5.23×10^5, 6.17×10^5, 4.64×10^5	25.35, 25.80, 26.65
Misalignment of accelerometer triad (arc-sec)	27.12, 27.69, 27.85	2.17×10^5, 3.37×10^5, 2.85×10^5	9.91, 9.99, 10.24
Biases of accelerometers (μg)	35.75, 36.89, 36.87	2.66×10^5, 3.09×10^5, 4.68×10^5	20.53, 20.63, 20.36

Table 6. Calibration results of both methods.

Parameters calibrated	Traditional method	Proposed method	Calibration discrepancies
Scale factors of accelerometers	33.390 707	33.390 492	−6.44 ppm
	33.446 630	33.446 452	−5.33 ppm
	31.476 791	31.476 642	−4.72 ppm
Misalignment of accelerometer triad (arc-sec)	−133.85	−133.10	0.75
	−124.05	−124.16	−0.11
	543.64	542.86	−0.78
Biases of accelerometers (μg)	−213.82	−220.29	−6.47
	−678.16	−698.54	−20.38
	1303.16	1299.53	−3.63
Scale factors of gyroscopes	$4.423\,985\,08 \times 10^5$	$4.423\,985\,30 \times 10^5$	0.05 ppm
	$4.422\,587\,58 \times 10^5$	$4.422\,587\,60 \times 10^5$	0.00 ppm
	$4.424\,270\,91 \times 10^5$	$4.424\,270\,87 \times 10^5$	−0.01 ppm
Misalignment of gyroscope triad (arc-sec)	16.60	1.42	−15.18
	153.40	165.34	11.94
	31.66	29.56	−2.10
Biases of gyroscopes ($^\circ$ h^{-1})	0.067 179	0.067 612	0.43×10^{-3}
	0.009 561	0.008 831	-0.73×10^{-3}
	−0.022 066	−0.022 647	-0.58×10^{-3}
Inter-triad misalignment angles between the gyroscope and accelerometer triads (arc-sec)	221.11	220.52	−0.59
	144.56	156.19	11.63
	51.01	66.10	15.09

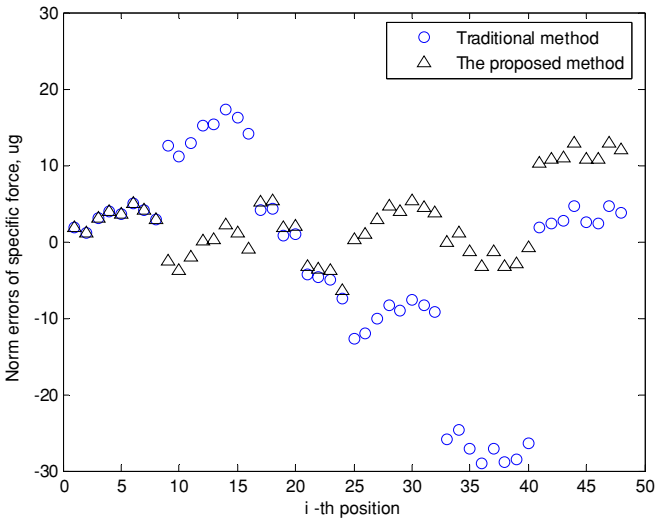

Figure 3. Norm errors of specific force measurement for static IMU.

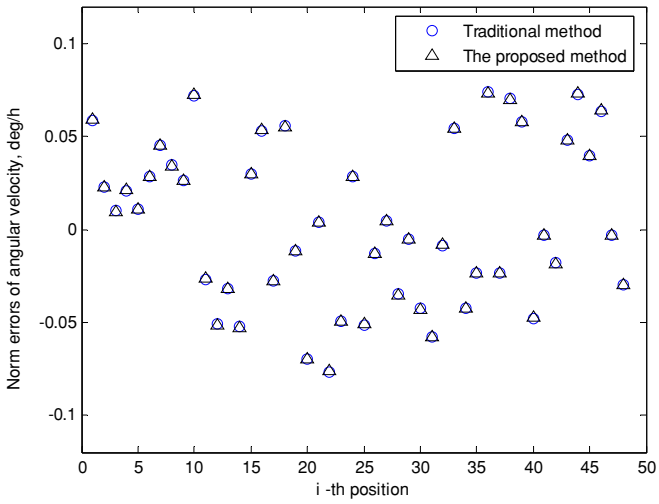

Figure 4. Norm errors of angular velocity for static IMU.

tests, the IMU was rotated to excite calibration parameter errors. Accelerometer and gyroscope measurements in test I are shown in figures 5 and 6 respectively, and navigation position errors are shown in figure 7 (the starting position is denoted by a star). Sequential rotations took place frequently in 8700 s. Accelerometer and gyroscope measurements in test II are shown in figures 8 and 9, respectively, and figure 10 gives the navigation position errors. Test II lasted for 8400 s, and only three rotations took place along the same axis in the

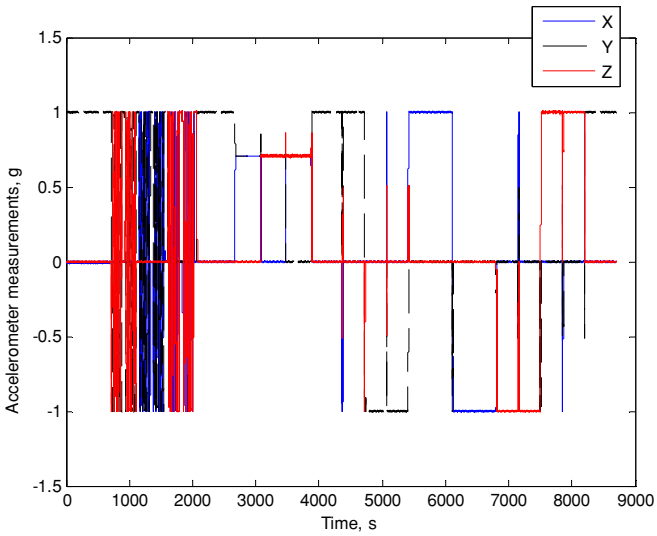

Figure 5. Accelerometer measurements in test I.

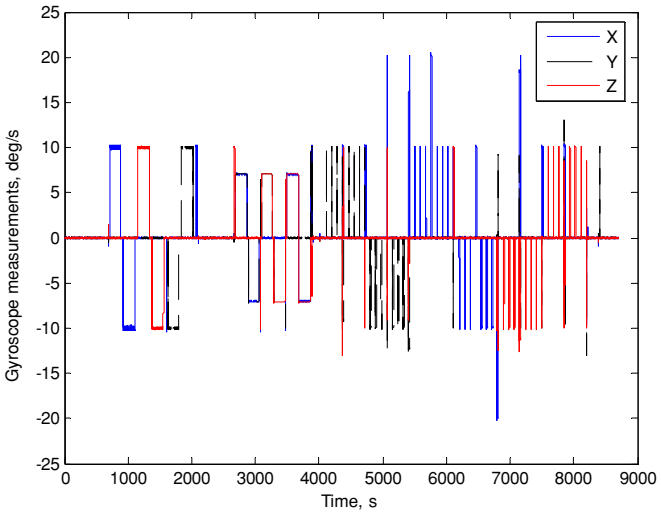

Figure 6. Gyroscope measurements in test I.

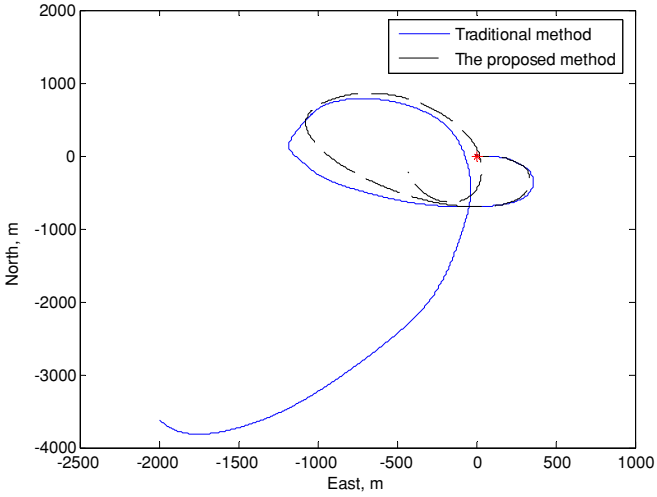

Figure 7. Navigation position errors of test I. (The starting position is denoted by a star.)

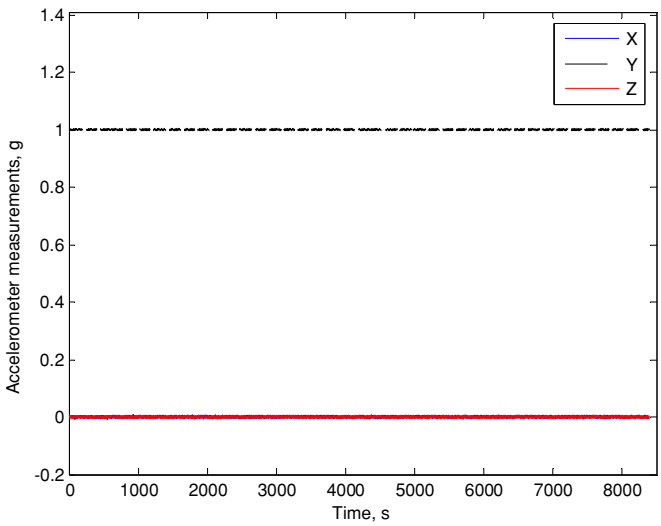

Figure 8. Accelerometer measurements in test II.

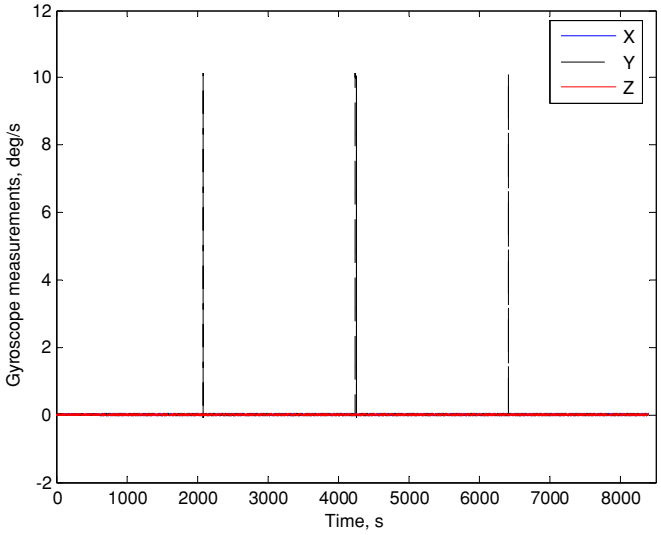

Figure 9. Gyroscope measurements in test II.

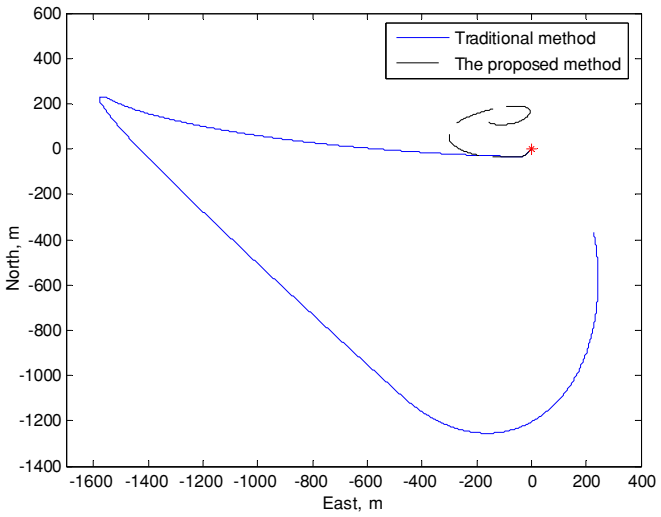

Figure 10. Navigation position errors of test II. (The starting position is denoted by a star.)

test. Figures 7 and 10 show that parameters by the proposed method are remarkably better than those by the traditional method, notably for a navigational grade IMU.

6. Conclusion

Calibration of the IMU is a necessary phase of inertial navigation. The so-called multi-position calibration is based on the fact that the norms of the measured outputs of the accelerometer and gyroscope cluster are equal to the magnitudes of the specific force and rotational velocity inputs, respectively. This paper investigates two important open issues: calibration of inter-triad misalignment between the gyroscope and accelerometer triads and the optimal calibration scheme design. Using the rotational axes measurements separately derived by the gyroscope and accelerometer triads, we propose a new approach to calibrate the inter-triad misalignment. By maximizing the sensitivity of the norm of the IMU measurement to the calibration parameters, we propose an approximately optimal calibration scheme. Simulations verify the feasibility and effectiveness. The improved multi-position approach was used to calibrate a navigation grade IMU. Static measurement tests and inertial navigation tests show that the new approach outperforms the traditional laboratory calibration method, meanwhile relaxing the requirement of precise orientation control.

Acknowledgments

We thank the PhD students Yangming Huang and Jie Yang for their help in real tests. This work was supported in part by National Natural Science Foundation of China (60604011) and Foundation for the Author of National Excellent Doctoral Dissertation of PR China (FANEDD 200897).

References

[1] Titterton D H and Weston J L 2004 *Strapdown Inertial Navigation Technology* (London: Peter Peregrinus on behalf of the Institute of Electrical Engineers)

[2] Niu X 2002 Micromachined attitude measurement unit with application in satellite TV antenna stabilization *PhD Dissertation* Department of Precision Instruments and Machinery, Tsinghua University

[3] Shin E-H 2001 Accuracy improvement of low cost INS/GPS for land applications *MSc Dissertation* Department of Geomatics Engineering, University of Calgary, Calgary

[4] Skog I and Handel P 2006 Calibration of a MEMS inertial measurement unit *IMEKO XVII World Congress, Metrology for a Sustainable Development (Rio de Janeiro, Brazil)*

[5] Frosio I, Stuani S and Borghese N A 2006 Autocalibration of MEMS accelerometer *IEEE Instrumentation and Measurement Technology Conf. (Sorrento, Italy)*

[6] Syed Z F, Aggarwal P, Goodall C, Niu X and El-Sheimy N 2007 A new multi-position calibration method for MEMS inertial navigation systems *Meas. Sci. Technol.* **18** 1897–907

[7] Fong W T, Ong S K and Nee A Y C 2008 Methods for in-field user calibration of an inertial measurement unit without external equipment *Meas. Sci. Technol.* **19** 085202

[8] Zhang H, Wu Y, Wu M, Hu X and Zha Y 2008 A multi-position calibration algorithm for inertial measurement units *AIAA Guidance, Navigation and Control Conf. and Exhibit (Honolulu, HI)*

[9] Artese G and Trecroci A 2008 Calibration of a low cost MEMS INS sensor for an integrated navigation system *Int. Archives of the Photogrammetry, Remote Sensing and Spatial Information Sciences (Beijing)*

[10] Sahawneh L and Jarrah M A 2008 Development and calibration of low cost MEMS IMU for UAV applications *5th Int. Symp. on Mechatronics and Its Applications (Amman, Jordan)*

[11] Kim K, Sun Y, Voyles R M and Nelson B J 2007 Calibration of multi-axis MEMS force sensors using the shape-from-motion method *IEEE Sensors J.* **7** 344–51

[12] Hwangbo M and Kanade T 2008 Factorization-based calibration method for MEMS inertial measurement unit *IEEE Int. Conf. on Robotics and Automation (Pasadena, CA, USA)*

[13] Chatfield A B 1997 *Fundamentals of High Accuracy Inertial Navigation* (Reston, VA: American Institute of Aeronautics and Astronautics)

[14] Nahi N E and Napjus G A 1971 Design of optimal probing signals for vector parameter estimation *IEEE Conf. on Decision and Control (Miami, FL)* Preprints

[15] Kalaba R E and Spingarn K 1973 Optimal inputs and sensitivities for parameter estimation *J. Optim. Theory Appl.* **11** 56–67

[16] Mehra R K 1974 Optimal inputs for linear system identification *IEEE Trans. Autom. Control* **19** 192–200

[17] Kalaba R E and Spingarn K 1978 On the numerical determination of optimal inputs *J. Optim. Theory Appl.* **25** 219–27

[18] Shuster M D and Oh S D 1981 Three-axis attitude determination from vector observations *J. Guid. Control Dyn.* **4** 70–7

[19] Xiao L, Wei S and Sun W 2008 Research on the high accuracy rapid test method of IMU *Chin. J. Astronaut.* **29** 172–7 (in Chinese)